ACS APPLIED NANO MATERIALS

www.acsanm.org Article

Heating-Induced Transformation of Anatase TiO_2 Nanorods into Rock-Salt TiO Nanoparticles: Implications for Photocatalytic and Gas-Sensing Applications

Xiaodan Chen,* Seyed Naveed Hosseini, and Marijn A. van Huis*

Cite This: *ACS Appl. Nano Mater.* 2022, 5, 1600−1606 Read Online

ACCESS | Metrics & More | Article Recommendations | Supporting Information

ABSTRACT: Anatase TiO_2 nanocrystals (NCs) play a vital role in photocatalytic applications due to their high catalytic activity and in gas-sensing applications due to their high chemical sensitivity. Here, we report the transformation at elevated temperature of anatase nanorods (NRs) with a length of 25 nm into rock-salt TiO nanoparticles with an average size of 9.2 ± 2.1 nm investigated by means of in situ heating in the transmission electron microscope. The NRs were completely transformed to titanium monoxide NCs after heating to a temperature of 1200 °C. We also identified an intermediate stage in the temperature range of 950−1200 °C, during which not only the anatase and rock-salt phases were found but also the brookite phase. Understanding of the phase and morphology evolution at high temperatures is of essence to the functionality of the NRs in various applications, as discussed in this work. Moreover, the high-temperature transformation to titanium monoxide is of interest as rock-salt TiO (γ-TiO) is known to exhibit superconducting properties. We propose the heating-induced transformation as a physical route to synthesize TiO NCs of very small size.

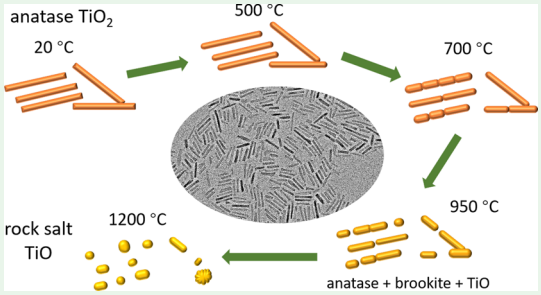

KEYWORDS: *anatase titanium dioxide, nanorods, phase transformation, in situ electron microscopy, titanium monoxide*

1. INTRODUCTION

Titanium dioxides have been studied for more than half a century, and the investigation of their nanostructural forms is continuously intensifying.[1−6] The interest in nanoscale TiO_2 stems from its natural abundance, non-toxicity, high stability, and advanced functional properties including, in particular, its very effective application as a photocatalyst.[7−11] It is one of the very few materials that is capable of light-induced water splitting without the need of adding any fuel to drive the reaction.[12] It can also be used for the conversion of solar energy to electric power[13] and for the degradation of highly toxic materials and pollutants.[14] Because of the high photocatalytic performance, TiO_2 also has potential to be used as an anti-bacterial and for self-cleaning coating of high-temperature process ceramics.[11,15−20] Moreover, TiO_2 and also TiO_2-based composites are also suitable gas sensor materials in electronic devices, which are based on surface oxygen vacancy formation, selective ion absorption, or desorption mechanisms.[21−24]

In contrast to bulk TiO_2 materials, TiO_2 nanoparticles have the advantage of a high surface-to-volume ratio. Consequently, the nanoparticles have much higher adsorption ability than the bulk material, leading to a high reactivity in photocatalytic and gas-sensing applications.[25] Also, the morphology of the nanoscale particles is of major importance and results in different performances.[6] It is reported that the nanorods (NRs) have a higher interfacial charge carrier transfer rate and density of active sites available for surface reactions in comparison to spherical particles, which is due to the even higher surface-to-volume ratio of the rod-like shape.[26] The anatase NRs investigated in this study are also proper candidates for serving as building blocks for liquid crystals due to their shape and orientation-dependent collective properties, which has been demonstrated already for brookite NRs.[27] The morphology, size, and crystal structure of the particles are directly related to their functional properties such as catalytic and (opto)-electrical properties, determining the range of applicable operation temperatures. For applications in gas sensors and antibacterial coatings, the desired operation temperatures can be very high. Consequently, the thermal behavior and temporal stability of TiO_2 NRs are of major importance to their performance, and here, we investigate the thermal evolution of anatase NRs by in situ heating in transmission electron microscopy (TEM).

There are three phases of TiO_2 that predominantly occur in nature: rutile, anatase, and brookite. All three phases are composed of TiO_6 octahedra with different Ti−O bond

Received: December 15, 2021
Accepted: December 27, 2021
Published: January 7, 2022

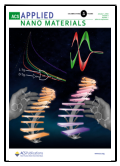

lengths. Their schematic crystal structures are shown in Figure 1 and detailed crystallographic data are provided in Table 1.

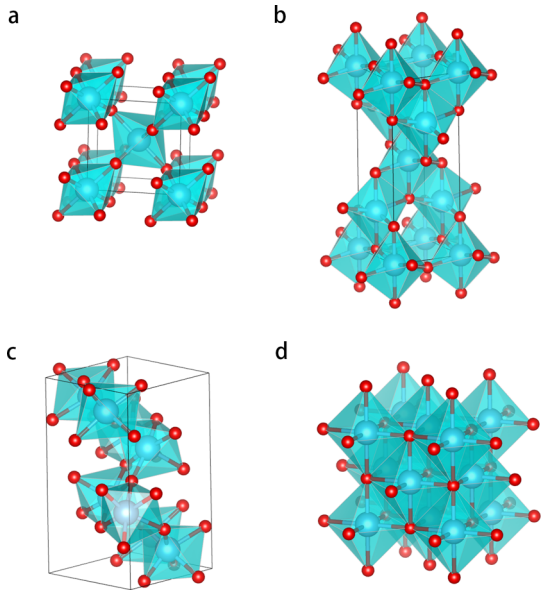

Figure 1. Structure of the TiO_x polymorphs: (a) rutile, (b) anatase, (c) brookite, and (d) γ-TiO (rock salt). Ti atoms are represented by blue spheres, and O atoms are represented by red spheres.

Table 1. Structure, Space Group, and Lattice Constant of Rutile, Anatase, Brookite, and γ-TiO

	structure	space group	lattice parameter (Å)[3,44]
rutile	tetragonal	$P4_2/mnm$ (136)	$a = b = 4.593$; $c = 2.959$
anatase	tetragonal	$I4_1/amd$ (141)	$a = b = 3.785$; $c = 9.514$
brookite	orthorhombic	$Pbca$ (61)	$a = 9.184$; $b = 5.447$; $c = 5.145$
γ-TiO	cubic	$Fm\bar{3}m$ (225)	$a = b = c = 4.24$

Rutile is the most stable phase in the bulk form, while the anatase phase is reported to have the highest photocatalytic activity.[10,28] Many studies show the irreversible transformation from anatase or brookite to the rutile phase.[28−33] However, the properties at the nanoscale are different. It has been shown that the anatase phase is preferred for nanoparticles.[34−38] The stability and phase transformation between the polymorphs were reported to depend on several factors, such as temperature, pH,[34] synthesis method,[18−20] and presence of impurities.[39,40] Moreover, the shape of the particles could be also manipulated during synthesis.[18,27,41] It is also possible to enhance the adsorption properties of the nanocrystals (NCs) by exposing different facets.[34,42] The shape of the NC is therefore important to take into consideration during investigation of the phase stability of TiO_2 NCs. The transformations between different polymorphs result in changes in their chemical and physical properties, which consequently affects their functionality in applications.[43,44]

Apart from the phase transformation between titanium dioxides, the transformation to titanium monoxides is also reported in several studies.[45−47] Titanium monoxides have been observed in four different phases, of which rock-salt cubic TiO (also named γ-TiO) is the stable phase at high temperature.[48−50] It has been shown that TiO has superconducting properties.[51−53] TiO thin films were successfully fabricated by ion bombardment-induced chemical reduction, laser hydrothermal reductive ablation, and other methods.[45,51,54] Nanopowders of TiO have been synthesized previously, for example, by ball milling, fragmentation, and other methods.[55−58] The typical size of the nanoparticles obtained in those powders is quite large, although in the order of ∼100 nm or larger. Simon et al. have successfully synthesized N-doped cubic TiO nanoparticles with a size below 10 nm by laser pyrolysis.[59] In that study, it was reported that apart from the N doping, carbon contamination was also introduced during the synthesis and that post-synthesis annealing was required to whiten the samples. In the present work, we have obtained pure TiO NCs with a typical size of ∼10 nm or smaller.

Here, we investigate the thermal evolution of anatase TiO_2 NRs using in situ TEM where superior resolution in the electron microscope during heating is obtained by employing micro-electro-mechanical systems (MEMS) technology, allowing to monitor chemical and physical transitions of nanoparticles in real-time and at the atomic scale.[60,61] In order to avoid any influence of the electron beam on the observations, the field of view in the TEM was often changed to areas not previously exposed to the electron beam, as detailed in the Experimental Section. Thermal evolution was observed to take place everywhere on the heating chip. The anatase NRs fully transformed to rock-salt TiO at 1200 °C, with an intermediated stage appearing from 950 °C onward. At the intermediate stage, a mixture of the anatase, brookite, and rock-salt phases was found. The thermal stability of anatase NRs is of importance for their implementation in applications. Furthermore, the transformation elucidated in this paper may serve as a route toward obtaining rock-salt titanium monoxide (TiO) nanoparticles of very small size.

2. EXPERIMENTAL SECTION

2.1. Synthesis. Titanium (IV) isopropoxide or TTIP ($Ti(OCH(CH_3)_2)_4$, 97.0%), oleic acid (OLAC, 90%), acetone, and toluene were purchased from Sigma−Aldrich and used as received. All experimental procedures were carried out either in an inert atmosphere using a standard Schlenk line setup or in a glove box. The anatase titanium dioxide NRs were synthesized following a slightly modified version of the synthesis described in the literature by Joo et al.,[62] where OLAC was used as the solvent, reagent, and ligand. In a typical synthesis, OLAC (100.0 mmol, 31.6 mL) was degassed in a 250 mL three-neck round bottom flask at 120 °C for an hour under vacuum and vigorous stirring. Then, the flask was cooled down under vacuum to 40 °C, followed by switching to nitrogen and the swift addition of TTIP (34.0 mmol, 10 mL), which was prepared in the glove box in advance. The mixture was then heated up to 250 °C in 20 min and kept at this temperature for 2 h. Caution should be taken as the reaction is rather violent with concomitant release of gases and foam formation expanding in the flask and should be controlled by nitrogen overflow/pressure as well as an extra needle as an outlet in a septum on one of the necks of the flask. After thermal fluctuations at high temperatures, the yellow solution gradually turned into a white−gray foam and finally a gray solution. The heating mantle was then removed after 2 h, and the flask was allowed to cool to room temperature. A size-selective precipitation process was performed on the as-synthesized TiO_2 NCs to separate TiO_2 NRs. Thus, the dispersion of the TiO_2 NCs was centrifuged at 6000 rcf (relative centrifugal force) for 10 min and then NR precipitations were redispersed in toluene. The washing step was repeated at least two times to achieve optically clear dispersions of TiO_2 NRs. The dimension of the NRs was on average 3.6 ± 0.3 nm (diameter) and 24.6 ± 3.4 nm (length).

https://doi.org/10.1021/acsanm.1c04346
ACS Appl. Nano Mater. 2022, 5, 1600−1606

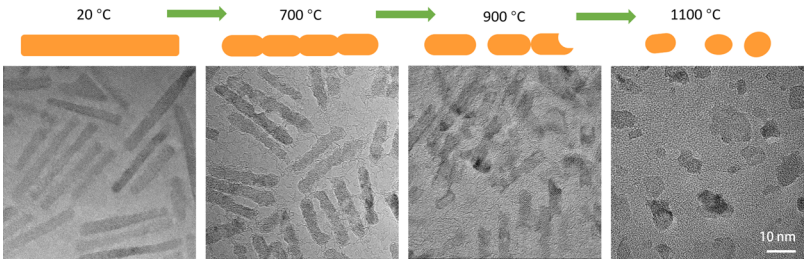

Figure 2. Schematic process and high-resolution TEM images of TiO_x NCs during heating. At 700 °C, the surfaces of the NRs deformed. At 900 °C, the NRs broke up, and sometimes the neighboring rods coalesced. Upon heating to 1000 °C, most NRs transformed to smaller nanoparticles.

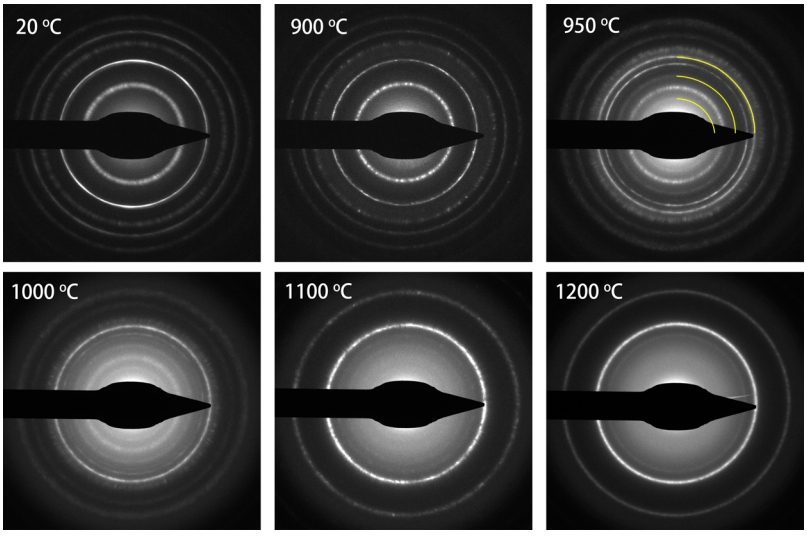

Figure 3. SADPs of the titanium oxide NRs during heating. At room temperature and up to 900 °C, the patterns correspond to the anatase crystal structure. At 950 °C, a new phase started to form, as indicated by the yellow arcs. At the temperature of 1200 °C, all nanoparticles had transformed to rock-salt TiO, which, because of the high symmetry of this phase, only has few rings in the SADP.

2.2. X-ray Diffraction Characterization. The crystal structure of TiO_2 NRs in pristine samples was confirmed by X-ray diffraction (XRD) measurements. XRD was performed using a Bruker-AXS D2 Phaser X-ray diffractometer with Co Kα radiation (λ = 1.79026 Å) operated at 30 kV and 10 mA.

2.3. TEM Characterization. All in situ TEM investigations on the anatase NRs were conducted using an FEI TalosF200X TEM instrument operating at 200 kV. High-resolution high-angle annular dark-field scanning transmission electron microscopy (HAADF-STEM) images of the rock-salt TiO nanoparticles obtained after heating were recorded with a double aberration-corrected TFS Spectra 300 TEM instrument operating at 300 kV. The specimens were prepared by drop casting the anatase TiO_2 NRs solution onto the MEMS heating chip. This chip was subsequently mounted on a dedicated in situ heating TEM holder from DENSsolutions.

The TiO_2 specimens were first heated from 20 to 1200 °C with 100 °C increments. The heating profile is shown in Figure S1 of the Supporting Information (SI). The nanoscale phase transformation started around 900 °C. In a second heating experiment, the specimen was heated from 20 to 900 °C with 100 °C increments, but with smaller increments of 50 °C when raising the temperature further from 900 to 1100 °C, in order to monitor the transformations more closely.

The inspected area of the sample was changed very often to areas not previously exposed to the electron beam in order to exclude any possible beam-induced effects. The transformations reported in this work were found to occur everywhere on the heating chip, also in areas not previously exposed to the electron beam. Furthermore, serving as a reference measurement and in order to fully exclude any electron beam effects, the samples were also heated ex situ outside of the TEM. For these ex situ experiments, the samples were heated with the heating holder inserted in a high vacuum chamber (Gatan pumping station model 655), applying the same heating rate as in the in situ heating experiments. The pressure in the high vacuum chamber was approximately 1.0×10^{-3} ~10^{-4} Pa. After holding the temperature at 1200 °C for 15 min, the sample was cooled down fast to room temperature and swiftly inserted in the TEM for subsequent analysis.

3. RESULTS AND DISCUSSION

A TEM micrograph of the pristine as-synthesized samples is shown in the left panel of Figure 2. The NRs have a length of 24.6 ± 3.4 nm and a diameter of 3.6 ± 0.3 nm. Most of the NRs have sharp edges at room temperature. An XRD spectrum confirming the anatase phase is shown in Figure S2. These anatase TiO_2 NRs were heated from room temperature to 1200 °C following the procedure mentioned in the Experimental Section. The field of view was often changed during the in situ experiments to verify that the transformations took place everywhere, also in areas that had not been previously exposed to the electron beam. Figure 2 shows high-resolution images and schematic panels of the thermal evolution of specimens from room temperature to 1100 °C. The morphology of the specimens changed during heating. Upon heating to 500 °C, the edges became rounded. Most likely, the oleic acid ligands degrade at this temperature resulting in destabilization of the NR surfaces. At 700 °C, the surfaces of the NRs deformed more and were no longer smooth. At 900 °C, some NRs broke up into multiple

https://doi.org/10.1021/acsanm.1c04346
ACS Appl. Nano Mater. 2022, 5, 1600−1606

segments and were partly sublimated, while sometimes neighboring rods had coalesced. Upon heating to 1000 °C, most NRs had transformed into smaller nanoparticles. Images with lower magnification and more temperature steps during heating are shown in Figure S3.

Figure 3 shows the selected area diffraction patterns (SADPs) of the specimens during heating. Up to 900 °C, the diffraction pattern (DP) corresponded to that of the anatase crystal structure. When the temperature was raised to 950 °C, a few more rings appeared (marked by the yellow arcs), indicating the formation of a new structure that is neither anatase TiO_2 nor cubic TiO. The indexing of this new phase will be discussed below. With further increase in the temperature, the inner rings disappeared gradually. At 1200 °C, only three rings remained. The rings were indexed and found to correspond to the cubic γ-TiO structure. This means that the anatase TiO_2 NRs were finally reduced to rock-salt TiO. High-resolution STEM images shown in Figure 4 confirm

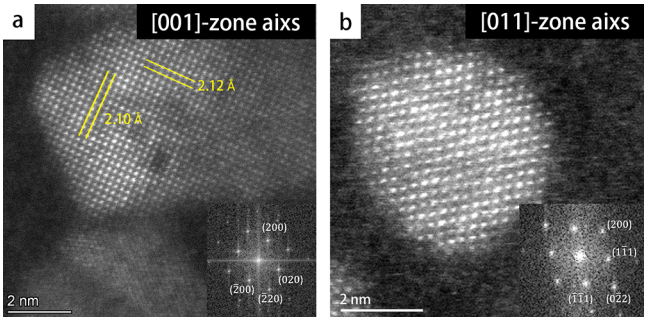

Figure 4. High-resolution STEM images of two γ-TiO NCs recorded after heating to 1200 °C. Corresponding fast-Fourier transform patterns are shown as insets, where the cubic TiO structure in (a) is oriented in the [001]-zone axis and (b) in the [011]-zone axis, respectively. The scale bar in both images indicates 2 nm.

the cubic TiO structure. The average size of the TiO particles is determined to be 9.2 ± 2.1 nm (based on the measurement of the dimensions of 200 nanoparticles). A histogram of the size distribution is shown in Figure S4.

In order to resolve the detailed phase transformation process between 950 and 1200 °C, the DP at 950 °C was measured and compared with the DP at 900 °C which corresponds to the anatase structure (shown in Figure 5a). The rings that additionally appeared at 950 °C are indicated in yellow (#1, 3, 5), and the rings corresponding to the anatase structure are marked in red (#2, 4, 6−8). The DPs at 20, 900, 950, 1000, and 1200 °C were integrated and are shown in Figure 5b.

The integrated DPs at 900 and 20 °C both show the anatase structure, while at 950 °C, there are three new peaks, marked as no. 1, 3, and 5 (corresponding to the new rings in the DP). With increasing temperature, ring no. 5 remains while the other peaks disappear gradually during further heating to a temperature of 1200 °C (also shown in Figure S5). In the DP recorded at 950 °C, peak no. 1 corresponds to a lattice spacing of 4.59 Å, which is a rather big value for lattice spacing but which corresponds very well to the (200)-reflection of the brookite phase. Moreover, ring no. 3 corresponds to a lattice spacing of 2.90 Å, corresponding to the (211)-reflection of brookite. The DP of the specimens at 950 °C was also compared to the as-synthesized brookite NRs at 20 °C (synthesized with the same method as the previous work[27]). From the comparison (shown in Figure S6), most of the rings

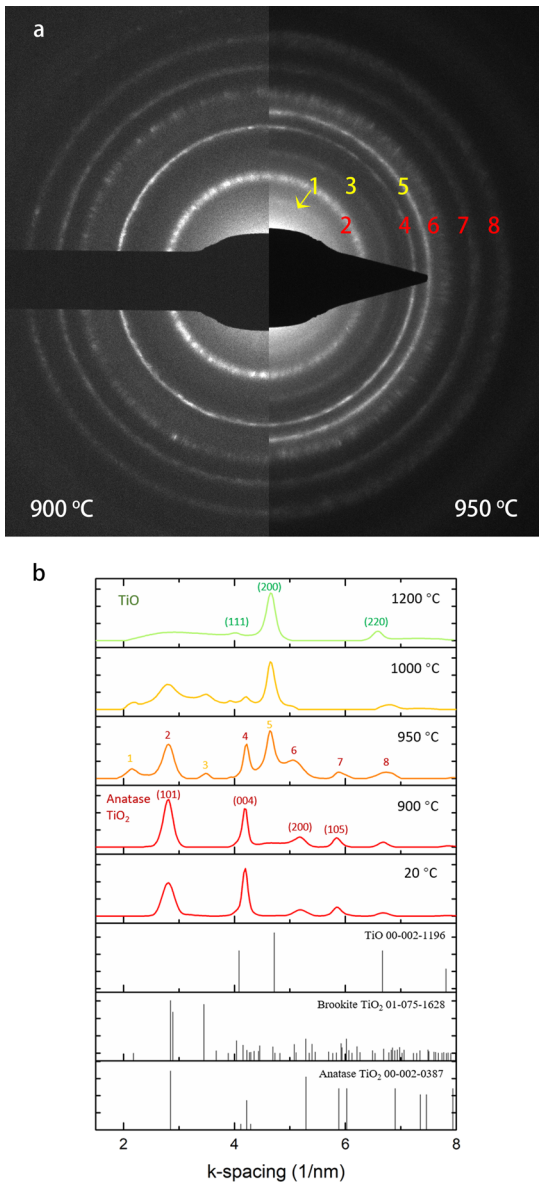

Figure 5. Comparison of SADPs at different temperatures to show phase transformation. (a) Comparison of SADPs at 900 °C (left) and 950 °C (right) and (b) comparison of integrated DPs at 20, 900, 950, 1000, and 1200 °C. The peaks at 950 °C are marked the same color as that of the corresponding rings in the DP. The XRD reference spectra of anatase, brookite, and cubic TiO are shown at the bottom.

in the DP of the specimen at 950 °C could be related to the corresponding rings in the DP of brookite, except for rings no. 4 and 5 while Figure 5b shows that ring no. 4 corresponds to the (004) reflection of anatase and ring no. 5 corresponds to the (200) reflection of TiO. This indicates that anatase TiO_2, brookite TiO_2, and cubic TiO all existed in the temperature range between 950 and 1000 °C. After heating to 1100 °C and at 1200 °C, only the cubic TiO phase remained.

The NRs remained in the anatase phase up to a temperature of 950 °C, which is different from the phase diagram shown in the paper by Murray and Wriedt,[49] who reported that anatase will transform to rutile at a temperature of about 600 °C in vacuum. The difference between their and our findings can be explained by the small size of the NRs. The research of Naicker et al.[63] showed that in the nanoscale range, the surface energy

https://doi.org/10.1021/acsanm.1c04346
ACS Appl. Nano Mater. 2022, 5, 1600−1606

of anatase and brookite is smaller than that of rutile nanospheres with the same size. For nanospheres larger than 4 nm, the surface energy of brookite tends to be smaller than that of anatase. The smaller surface energy of brookite could explain the transformation of anatase in this work to brookite instead of rutile at high temperature.

To verify that the transformation to TiO also takes place at high concentrations of anatase NRs, a larger amount of sample was drop-cast on a heating chip and heated in situ to a temperature of 1200 °C. The result is displayed in Figure S7. In particular, from the SADP in panel (a) it is also clear that when a large amount of NRs is heated, the anatase NRs fully transform to rock-salt TiO. From the TEM images in panels (b,c), it is clear that part of the material has sublimated, and some of the material has aggregated. The only difference with the heating results of the low-concentration deposited samples is that for the high-concentration deposited sample, the average TiO particle size after heating is larger than that in the experiments where only a monolayer or less of anatase nanoparticles is drop-cast.

Ex situ heating was conducted as a reference measurement and to further exclude the effect of electron illumination. NRs were heated by using the heating holder inserted in a vacuum chamber instead of in the TEM instrument (see Experimental Section for details). After heating to 1200 °C, the sample was cooled down and moved to the microscope for electron diffraction analysis and EM characterization. The DP after ex situ heating is shown in Figure S8, in which peaks corresponding to anatase, rutile, and TiO are all detected. This means that, when heating outside the microscope, the transformation to TiO is not complete. Some of the sample remained in the anatase phase, and some of it transformed to rutile. The (partial) transformation to rutile can be expected under conditions of heating to high temperatures (1200 °C) while the oxygen partial pressure is not sufficiently low, as will be discussed in more detail below.

Appearance of the rutile phase upon heating of anatase or brookite nanoparticles has been reported in previous works. Koparde and Cummings[64] investigated the phase transformation between anatase and rutile by molecular dynamics (MD) simulations. Their results show that nanoparticles larger than 1.65 nm are stable as rutile. They found that when anatase was sintered with amorphous TiO_2, a brookite agglomerate was obtained. They also expressed the expectation that brookite would transform to rutile with a longer simulation time. Mao et al.[65] investigated the sintering-induced phase transformation from anatase to brookite at 1200 °C with MD and also predicted the further transformation to rutile. All their prediction of the formation of brookite is in good agreement with our observation of brookite as the intermediate phase during the in situ experiment. Moreover, the final transformation to rutile is in agreement with the ex situ heating results. We mention here that the force-field molecular dynamics simulations, in general, are not suited for the simulation of chemical transitions where the valence state of the metal ions changes. That in our case a transformation to cubic TiO took place rather than further transformation to rutile, can be plausibly explained by the low-pressure experimental conditions associated with heating in the electron microscope, as discussed in our recent work on the transformation of Co_3O_4 to CoO nanoparticles.[61] The temperature at which dissociation reactions take place is in general strongly dependent on the partial oxygen pressure, also when the total pressure and, therefore, the partial oxygen pressure (always expressed with respect to the standard pressure) are low.[66] In the present case, the dissociation reaction is TiO_2 (anatase) → TiO + $1/2O_2$. In the vacuum inside the column of the TEM, oxygen atoms are continuously removed from the system, yielding a very low partial oxygen pressure, thereby driving the transformation to a phase with lower oxygen content, which here is γ-TiO. When the heating took place in the vacuum chamber, the overall pressure (about 10^{-3} Pa) is not as low as that in the microscope (about 10^{-6} Pa). Consequently, the partial oxygen pressure (which is at most equal to the overall pressure in vacuum chambers) will be considerably lower in the TEM column than in the ex situ vacuum chamber. The different oxygen partial pressure in the ex situ chamber is most likely the reason that only part of the sample transformed to TiO while some of the nanoparticles transformed to rutile. Rutile is the most stable phase for TiO_2 in general and will be eventually formed when the transformation to TiO does not fully take place.

The structural transformation to TiO will be accompanied by a drastic change in physical and chemical properties, as anatase TiO_2 is a well-known semiconductor, while rock-salt TiO is known to be metal and even a superconductor at low temperature.[51−53] It is clear that photocatalytic and gas-sensing functionalities are lost when the TiO_2 NRs transform to rock-salt TiO, as TiO is metallic (a conductor), while both for photocatalysis and gas-sensing, a semiconductor nature of the material is required. The metallic rock-salt TiO nanoparticles may have merit as catalytic particles for other chemical reactions; however, to the best of our knowledge, possible catalytic properties of nanoscale rock-salt TiO are yet to be explored.

4. CONCLUSIONS

In this study, anatase TiO_2 NRs were heated from room temperature to 1200 °C. The morphology of anatase NRs was found to be stable up to a temperature of 700 °C, after which the surface of NRs became uneven and the shape started to deform. From 900 °C, the NRs break up into smaller nanoparticles and sometimes coalesce. Therefore, for application under high-temperature conditions for either photocatalysis or gas-sensing, anatase NRs can be considered to be structurally stable and retain their functionality until 600 °C. Reduction to cubic γ-TiO was observed starting at temperatures from 950 °C. All nanoparticles had completely reduced to γ-TiO at 1200 °C. In the temperature range between 950 and 1200 °C, not only did the brookite phase appear as an intermediate phase but also the NCs exhibiting this intermediate phase were completely reduced to γ-TiO after heating to 1200 °C. The size range of 9.2 ± 2.1 nm of the rock-salt TiO NCs is an order of magnitude smaller than that of TiO nanopowders, and we propose the observed transformation mechanism as a physical route to the synthesis of TiO nanoparticles of very small size. The TiO NCs will not have photocatalytic or gas-sensing functionalities as these particles are metallic rather than semiconducting; however, the synthesis of nanoscale rock-salt TiO opens up opportunities for future investigations of their physical and chemical properties including electronic and catalytic functionalities.

Considering the applicability of photocatalysis and gas sensor devices based on anatase NRs, we infer from our analysis of the thermal evolution that their functionality is expected to be retained at operation temperatures up to 600

https://doi.org/10.1021/acsanm.1c04346
ACS Appl. Nano Mater. 2022, 5, 1600−1606

°C, while above that temperature, their functionality likely degrades. As mentioned, the functionalities of rock-salt TiO NCs are yet to be explored.

■ ASSOCIATED CONTENT

Supporting Information

The Supporting Information is available free of charge at https://pubs.acs.org/doi/10.1021/acsanm.1c04346.

Additional TEM images, SAED patterns, and histogram of the size distribution of TiO nanoparticles (PDF)

■ AUTHOR INFORMATION

Corresponding Authors

Xiaodan Chen − *Soft Condensed Matter, Debye Institute for Nanomaterials Science, Utrecht University, 3584 CC Utrecht, The Netherlands;* orcid.org/0000-0003-1005-8161; Email: x.chen1@uu.nl

Marijn A. van Huis − *Soft Condensed Matter, Debye Institute for Nanomaterials Science, Utrecht University, 3584 CC Utrecht, The Netherlands;* orcid.org/0000-0002-8039-2256; Email: m.a.vanhuis@uu.nl

Author

Seyed Naveed Hosseini − *Soft Condensed Matter, Debye Institute for Nanomaterials Science, Utrecht University, 3584 CC Utrecht, The Netherlands*

Complete contact information is available at: https://pubs.acs.org/10.1021/acsanm.1c04346

Author Contributions

X.C. performed all TEM and ED experiments, analyzed the results, and wrote the article. S.N.H. synthesized the anatase and brookite NRs and performed XRD measurements and analysis. M.A.v.H. supervised the project. All authors discussed and commented on the article.

Notes

The authors declare no competing financial interest.

■ ACKNOWLEDGMENTS

The authors acknowledge funding by the European Research Council through an ERC Consolidator grant (grant no. 683076). S.N.H. acknowledges the Dutch Technology Foundation STW (grant no. 14176), which is part of the Netherlands Organization for Scientific Research-Applied and Engineering Sciences (NWO-TTW) and partly funded by the Ministry of Economic Affairs. Figures of atomic structural models were produced using VESTA.[67] We thank Dr. Rafael Greogorio Mendes for help with the HR-STEM characterization. We thank Dennie Wezendonk for the X-ray measurements. We thank Prof. Alfons van Blaaderen, Dr. Arnout Imhof, and Dr. Patrick Baesjou for useful discussions.

■ REFERENCES

(1) Howard, C. J.; Sabine, T. M.; Dickson, F. Structural and Thermal Parameters for Rutile and Anatase. *Acta Crystallogr., Sect. B: Struct. Sci.* **1991**, *47*, 462−468.

(2) Meagher, E. P.; Lager, G. A. Polyhedral Thermal Expansion in the TiO_2 Polymorphs: Refinement of the Crystal Structures of Rutile and Brookite at High Temperature. *Can. Mineral.* **1979**, *17*, 77−85.

(3) Cromer, D. T.; Herrington, K. The Structures of Anatase and Rutile. *J. Am. Chem. Soc.* **1955**, *77*, 4708−4709.

(4) De Angelis, F.; Di Valentin, C.; Fantacci, S.; Vittadini, A.; Selloni, A. Theoretical Studies on Anatase and Less Common TiO_2 Phases: Bulk, Surfaces, and Nanomaterials. *Chem. Rev.* **2014**, *114*, 9708−9753.

(5) Breckenridge, R. G.; Hosler, W. R. Electrical Properties of Titanium Dioxide Semiconductors. *Phys. Rev.* **1953**, *91*, 793−802.

(6) Fazio, G.; Ferrighi, L.; Di Valentin, C. Spherical versus Faceted Anatase TiO_2 Nanoparticles: A Model Study of Structural and Electronic Properties. *J. Phys. Chem. C* **2015**, *119*, 20735−20746.

(7) Henderson, M. A. A surface science perspective on TiO_2 photocatalysis. *Surf. Sci. Rep.* **2011**, *66*, 185−297.

(8) Fujishima, A.; Zhang, X.; Tryk, D. TiO_2 Photocatalysis and Related Surface Phenomena. *Surf. Sci. Rep.* **2008**, *63*, 515−582.

(9) Thompson, T. L.; Yates, J. T. Surface Science Studies of the Photoactivation of TiO_2 - New Photochemical Processes. *Chem. Rev.* **2006**, *106*, 4428−4453.

(10) Kavan, L.; Grätzel, M.; Gilbert, S. E.; Klemenz, C.; Scheel, H. J. Electrochemical and Photoelectrochemical Investigation of Single-Crystal Anatase. *J. Am. Chem. Soc.* **1996**, *118*, 6716−6723.

(11) Rashidzadeh, M. Synthesis of High-Thermal Stable Titanium Dioxide Nanoparticles. *Int. J. Photoenergy* **2008**, *2008*, 245981.

(12) Bak, T.; Nowotny, J.; Rekas, M.; Sorrell, C. C. Photo-Electrochemical Hydrogen Generation from Water Using Solar Energy. Materials-Related Aspects. *Int. J. Hydrogen Energy* **2002**, *27*, 991−1022.

(13) Grätzel, M. Photoelectrochemical Cells. *Nature* **2001**, *414*, 338−344.

(14) Carp, O. Photoinduced Reactivity of Titanium Dioxide. *Prog. Solid State Chem.* **2004**, *32*, 33−177.

(15) Periyat, P.; Naufal, B.; Ullattil, S. G. A Review on High Temperature Stable Anatase TiO2 Photocatalysts. *Mater. Sci. Forum* **2016**, *855*, 78−93.

(16) Cao, L.; Chen, D.; Wu, W.-Q.; Tan, J. Z. Y.; Caruso, R. A. Monodisperse Anatase Titania Microspheres with High-Thermal Stability and Large Pore Size (∼80 Nm) as Efficient Photocatalysts. *J. Mater. Chem. A* **2017**, *5*, 3645−3654.

(17) Kumaravel, V.; Rhatigan, S.; Mathew, S.; Bartlett, J.; Nolan, M.; Hinder, S. J.; Sharma, P. K.; Singh, A.; Byrne, J. A.; Harrison, J.; Pillai, S. C. Indium-Doped TiO_2 Photocatalysts with High-Temperature Anatase Stability. *J. Phys. Chem. C* **2019**, *123*, 21083−21096.

(18) Rao, B. M.; Roy, S. C. Anatase TiO_2 Nanotube Arrays with High Temperature Stability. *RSC Adv.* **2014**, *4*, 38133−38139.

(19) Pillai, S. C.; Periyat, P.; George, R.; McCormack, D. E.; Seery, M. K.; Hayden, H.; Colreavy, J.; Corr, D.; Hinder, S. J. Synthesis of High-Temperature Stable Anatase TiO_2 Photocatalyst. *J. Phys. Chem. C* **2007**, *111*, 1605−1611.

(20) Etacheri, V.; Seery, M. K.; Hinder, S. J.; Pillai, S. C. Oxygen Rich Titania: A Dopant Free, High Temperature Stable, and Visible-Light Active Anatase Photocatalyst. *Adv. Funct. Mater.* **2011**, *21*, 3744−3752.

(21) Rzaij, J. M.; Abass, A. M. Review on: TiO_2 Thin Film as a Metal Oxide Gas Sensor. *J. Chem. Rev.* **2020**, *2*, 114−121.

(22) Karunagaran, B.; Uthirakumar, P.; Chung, S. J.; Velumani, S.; Suh, E.-K. TiO_2 Thin Film Gas Sensor for Monitoring Ammonia. *Mater. Charact.* **2007**, *58*, 680−684 58 (8-9 SPEC. ISS.).

(23) Sertel, B. C.; Sonmez, N. A.; Kaya, M. D.; Ozcelik, S. Development of MgO:TiO_2 Thin Films for Gas Sensor Applications. Ceramics International. *Ceram. Int.* **2019**, *45*, 2917−2921 February 15.

(24) Li, Z.; Yao, Z.; Haidry, A. A.; Plecenik, T.; Xie, L.; Sun, L.; Fatima, Q. Resistive-Type Hydrogen Gas Sensor Based on TiO_2: A Review. *Int. J. Hydrogen Energy* **2018**, *43*, 21114−21132 Pergamon November.

(25) Barnard, A. S.; Zapol, P. Effects of Particle Morphology and Surface Hydrogenation on the Phase Stability of TiO_2. *Phys. Rev. B: Condens. Matter Mater. Phys.* **2004**, *70*, 235403.

(26) Cozzoli, P. D.; Kornowski, A.; Weller, H. Low-Temperature Synthesis of Soluble and Processable Organic-Capped Anatase TiO_2 Nanorods. *J. Am. Chem. Soc.* **2003**, *125*, 14539−14548.

(27) Hosseini, S. N.; Grau-Carbonell, A.; Nikolaenkova, A. G.; Xie, X.; Chen, X.; Imhof, A.; Blaaderen, A.; Baesjou, P. J. Smectic Liquid

Crystalline Titanium Dioxide Nanorods: Reducing Attractions by Optimizing Ligand Density. *Adv. Funct. Mater.* **2020**, *30*, 2005491.
(28) Hanaor, D. A. H.; Sorrell, C. C. Review of the Anatase to Rutile Phase Transformation. *J. Mater. Sci.* **2011**, *46*, 855−874.
(29) Xu, W. X.; Zhu, S.; Fu, X. C.; Chen, Q. Structure of TiO_x Thin Film Studied by Raman Spectroscopy and XRD. *Appl. Surf. Sci.* **1999**, *148*, 253−262.
(30) Ren, R.; Yang, Z.; Shaw, L. L. Polymorphic Transformation and Powder Characteristics of TiO_2 during High Energy Milling. *J. Mater. Sci.* **2000**, *35*, 6015−6026.
(31) Valeeva, A. A.; Dorosheva, I. B.; Kozlova, E. A.; Kamalov, R. V.; Vokhmintsev, A. S.; Selishchev, D. S.; Saraev, A. A.; Gerasimov, E. Y.; Weinstein, I. A.; Rempel, A. A. Influence of Calcination on Photocatalytic Properties of Nonstoichiometric Titanium Dioxide Nanotubes. *J. Alloys Compd.* **2019**, *796*, 293−299.
(32) Li, K.; Xu, J.; Shi, W.; Wang, Y.; Peng, T. Synthesis of Size Controllable and Thermally Stable Rice-like Brookite Titania and Its Application as a Scattering Layer for Nano-Sized Titania Film-Based Dye-Sensitized Solar Cells. *J. Mater. Chem. A* **2014**, *2*, 1886−1896.
(33) Kominami, H.; Kohno, M.; Kera, Y. Synthesis of Brookite-Type Titanium Oxide Nano-Crystals in Organic Media. *J. Mater. Chem.* **2000**, *10*, 1151−1156.
(34) Barnard, A. S.; Curtiss, L. A. Prediction of TiO_2 Nanoparticle Phase and Shape Transitions Controlled by Surface Chemistry. *Nano Lett.* **2005**, *5*, 1261−1266.
(35) Zhang, H.; Banfield, J. F. Phase Transformation of Nanocrystalline Anatase-to-Rutile via Combined Interface and Surface Nucleation. *J. Mater. Res.* **2000**, *15*, 437−448.
(36) Gribb, A. A.; Banfield, J. F. Particle Size Effects on Transformation Kinetics and Phase Stability in Nanocrystalline TiO_2. *Am. Mineral.* **1997**, *82*, 717−728.
(37) Zhang, H.; Banfield, J. F. Thermodynamic Analysis of Phase Stability of Nanocrystalline Titania. *J. Mater. Chem.* **1998**, *8*, 2073−2076.
(38) Zhang, H.; Banfield, J. F. Understanding Polymorphic Phase Transformation Behavior during Growth of Nanocrystalline Aggregates: Insights from TiO_2. *J. Phys. Chem. B* **2000**, *104*, 3481−3487.
(39) Nie, X.; Zhuo, S.; Maeng, G.; Sohlberg, K. Doping of TiO_2 Polymorphs for Altered Optical and Photocatalytic Properties. *Int. J. Photoenergy* **2009**, *2009*, 294042.
(40) Bokhimi, X.; Morales, A.; Ortíz, E.; López, T.; Gómez, R.; Navarrete, J. Sulfate Ions in Titania Polymorphs. *J. Sol-Gel Sci. Technol.* **2004**, *29*, 31−40.
(41) Hu, W.; Li, L.; Li, G.; Tang, C.; Sun, L. High-Quality Brookite TiO_2 Flowers: Synthesis, Characterization, and Dielectric Performance. *Cryst. Growth Des.* **2009**, *9*, 3676−3682.
(42) Barnard, A. S.; Zapol, P.; Curtiss, L. A. Modeling the Morphology and Phase Stability of TiO_2 Nanocrystals in Water. *J. Chem. Theory Comput.* **2005**, *1*, 107−116.
(43) Bakardjieva, S.; Stengl, V.; Szatmary, L.; Subrt, J.; Lukac, J.; Murafa, N.; Niznansky, D.; Cizek, K.; Jirkovsky, J.; Petrova, N. Transformation of Brookite-Type TiO_2 Nanocrystals to Rutile: Correlation between Microstructure and Photoactivity. *J. Mater. Chem.* **2006**, *16*, 1709.
(44) Zhu, T.; Gao, S.-P. The Stability, Electronic Structure, and Optical Property of TiO_2 Polymorphs. *J. Phys. Chem. C* **2014**, *118*, 11385−11396.
(45) Pabón, B. M.; Beltrán, J. I.; Sánchez-Santolino, G.; Palacio, I.; López-Sánchez, J.; Rubio-Zuazo, J.; Rojo, J. M.; Ferrer, P.; Mascaraque, A.; Muñoz, M. C.; Varela, M.; Castro, G. R.; De La Fuente, O. R. Formation of Titanium Monoxide (001) Single-Crystalline Thin Film Induced by Ion Bombardment of Titanium Dioxide (110). *Nat. Commun.* **2015**, *6*, 6147.
(46) Hengerer, R.; Bolliger, B.; Erbudak, M.; Grätzel, M. Structure and Stability of the Anatase TiO_2 (101) and (001) Surfaces. *Surf. Sci.* **2000**, *460*, 162−169.
(47) Bouzoubaa, A.; Markovits, A.; Calatayud, M.; Minot, C. Comparison of the reduction of metal oxide surfaces: TiO2-anatase, TiO2-rutile and SnO2-rutile. *Surf. Sci.* **2005**, *583*, 107−117.
(48) Amano, S.; Bogdanovski, D.; Yamane, H.; Terauchi, M.; Dronskowski, R. ε-TiO, a Novel Stable Polymorph of Titanium Monoxide. *Angew. Chem.* **2016**, *128*, 1684−1689.
(49) Murray, J. L.; Wriedt, H. A. The O-Ti (Oxygen-Titanium) System. *J. Phase Equilib.* **1987**, *8*, 148−165.
(50) Bartkowski, S.; Neumann, M.; Kurmaev, E. Z.; Fedorenko, V. V.; Shamin, S. N.; Cherkashenko, V. M.; Nemnonov, S. N.; Winiarski, A.; Rubie, D. C. Electronic Structure of Titanium Monoxide. *Phys. Rev. B: Condens. Matter Mater. Phys.* **1997**, *56*, 10656−10667.
(51) Zhang, C.; Hao, F.; Gao, G.; Liu, X.; Ma, C.; Lin, Y.; Yin, Y.; Li, X. Enhanced Superconductivity in TiO Epitaxial Thin Films. *npj Quantum Mater.* **2017**, *2*, 2.
(52) Hulm, J. K.; Jones, C. K.; Hein, R. A.; Gibson, J. W. Superconductivity in the TiO and NbO Systems. *J. Low Temp. Phys.* **1972**, *7*, 291−307.
(53) Wang, D.; Huang, C.; He, J.; Che, X.; Zhang, H.; Huang, F. Enhanced Superconductivity in Rock-Salt TiO. *ACS Omega* **2017**, *2*, 1036−1039.
(54) Blazevska-Gilev, J.; Jandová, V.; Kupčík, J.; Bastl, Z.; Šubrt, J.; Bezdička, P.; Pola, J. Laser Hydrothermal Reductive Ablation of Titanium Monoxide: Hydrated TiO Particles with Modified Ti/O Surface. *J. Solid State Chem.* **2013**, *197*, 337−344.
(55) Nguyen, T.-T. -N.; He, J.-L. Preparation of Titanium Monoxide Nanopowder by Low-Energy Wet Ball-Milling. *Adv. Powder Technol.* **2016**, *27*, 1868−1873.
(56) Valeeva, A. A.; Petrovykh, K. A.; Schroettner, H.; Rempel, A. A. Effect of Stoichiometry on the Size of Titanium Monoxide Nanoparticles Produced by Fragmentation. *Inorg. Mater.* **2015**, *51*, 1132−1137.
(57) Wei, Y.; Shi, Y.; Zhang, X.; Li, D.; Zhang, L.; Gong, C.; Zhang, J. Preparation of Black Titanium Monoxide Nanoparticles and Their Potential in Electromagnetic Wave Absorption. *Adv. Powder Technol.* **2020**, *31*, 3458−3464.
(58) Valeeva, A. A.; Nazarova, S. Z.; Rempel, A. A. Influence of Particle Size, Stoichiometry, and Degree of Long-Range Order on Magnetic Susceptibility of Titanium Monoxide. *Phys. Solid State* **2016**, *58*, 771−778.
(59) Simon, P.; Pignon, B.; Miao, B.; Coste-Leconte, S.; Leconte, Y.; Marguet, S.; Jegou, P.; Bouchet-Fabre, B.; Reynaud, C.; Herlin-Boime, N. N-Doped Titanium Monoxide Nanoparticles with TiO Rock-Salt Structure, Low Energy Band Gap, and Visible Light Activity. *Chem. Mater.* **2010**, *22*, 3704−3711.
(60) Van Huis, M. A.; Young, N. P.; Pandraud, G.; Creemer, J. F.; Vanmaekelbergh, D.; Kirkland, A. I.; Zandbergen, H. W. Atomic Maging of Phase Transitions and Morphology Transformations in Nanocrystals. *Adv. Mater.* **2009**, *21*, 4992−4995.
(61) Chen, X.; Van Gog, H.; Van Huis, M. A. Transformation of Co_3O_4 nanoparticles to CoO Monitored by: In Situ TEM and Predicted Ferromagnetism at the Co_3O_4/CoO Interface from First Principles. *J. Mater. Chem. C* **2021**, *9*, 5662−5675.
(62) Joo, J.; Kwon, S. G.; Yu, T.; Cho, M.; Lee, J.; Yoon, J.; Hyeon, T. Large-Scale Synthesis of TiO_2 Nanorods via Nonhydrolytic Sol-Gel Ester Elimination Reaction and Their Application to Photocatalytic Inactivation of E. Coli. *J. Phys. Chem. B* **2005**, *109*, 15297−15302.
(63) Naicker, P. K.; Cummings, P. T.; Zhang, H.; Banfield, J. F. Characterization of Titanium Dioxide Nanoparticles Using Molecular Dynamics Simulations. *J. Phys. Chem. B* **2005**, *109*, 15243−15249.
(64) Koparde, V. N.; Cummings, P. T. Phase Transformations during Sintering of Titania Nanoparticles. *ACS Nano* **2008**, *2*, 1620−1624.
(65) Mao, Q.; Ren, Y.; Luo, K. H.; Li, S. Sintering-Induced Phase Transformation of Nanoparticles: A Molecular Dynamics Study. *J. Phys. Chem. C* **2015**, *119*, 28631−28639.
(66) Navrotsky, A.; Ma, C.; Lilova, K.; Birkner, N. Nanophase Transition Metal Oxides Show Large Thermodynamically Driven Shifts in Oxidation-Reduction Equilibria. *Science* **2010**, *330*, 199−201.
(67) Momma, K.; Izumi, F. VESTA 3 for Three-Dimensional Visualization of Crystal, Volumetric and Morphology Data. *J. Appl. Crystallogr.* **2011**, *44*, 1272−1276.

https://doi.org/10.1021/acsanm.1c04346
ACS Appl. Nano Mater. 2022, 5, 1600−1606